# Rate and State Friction Relation for Nanoscale Contacts: Thermally Activated Prandtl-Tomlinson Model with Chemical Aging

Kaiwen Tian,[1,*] David L. Goldsby,[2] and Robert W. Carpick[3,†]
[1]Department of Physics and Astronomy, University of Pennsylvania, Philadelphia, Pennsylvania 19104, USA
[2]Department of Earth and Environmental Sciences, University of Pennsylvania, Philadelphia, Pennsylvania 19104, USA
[3]Department of Mechanical Engineering and Applied Mechanics, University of Pennsylvania, Philadelphia, Pennsylvania 19104, USA

(Received 15 August 2017; published 2 May 2018; corrected 2 July 2018)

Rate and state friction (RSF) laws are widely used empirical relationships that describe macroscale to microscale frictional behavior. They entail a linear combination of the direct effect (the increase of friction with sliding velocity due to the reduced influence of thermal excitations) and the evolution effect (the change in friction with changes in contact "state," such as the real contact area or the degree of interfacial chemical bonds). Recent atomic force microscope (AFM) experiments and simulations found that nanoscale single-asperity amorphous silica-silica contacts exhibit logarithmic aging (increasing friction with time) over several decades of contact time, due to the formation of interfacial chemical bonds. Here we establish a physically based RSF relation for such contacts by combining the thermally activated Prandtl-Tomlinson (PTT) model with an evolution effect based on the physics of chemical aging. This thermally activated Prandtl-Tomlinson model with chemical aging (PTTCA), like the PTT model, uses the loading point velocity for describing the direct effect, not the tip velocity (as in conventional RSF laws). Also, in the PTTCA model, the combination of the evolution and direct effects may be nonlinear. We present AFM data consistent with the PTTCA model whereby in aging tests, for a given hold time, static friction increases with the logarithm of the loading point velocity. Kinetic friction also increases with the logarithm of the loading point velocity at sufficiently high velocities, but at a different increasing rate. The discrepancy between the rates of increase of static and kinetic friction with velocity arises from the fact that appreciable aging during static contact changes the energy landscape. Our approach extends the PTT model, originally used for crystalline substrates, to amorphous materials. It also establishes how conventional RSF laws can be modified for nanoscale single-asperity contacts to provide a physically based friction relation for nanoscale contacts that exhibit chemical bond-induced aging, as well as other aging mechanisms with similar physical characteristics.

DOI: 10.1103/PhysRevLett.120.186101

To describe friction at the macroscale, the rate and state friction (RSF) approach [1–14] is generally used by tribologists and geophysicists. While this family of relations is largely empirical in nature, they have found significant use as they often fit friction experimental results for many materials ranging from granular media [9,15] and rocks [1,3,5,9,16–18] to paper [16] and organic thin films [19–21].

For a macroscopic sliding block, the expression for the friction coefficient $\mu$ as a function of contact time $t$ and block velocity $v$ according to RSF laws is given by

$$\mu(t) = \mu_0 + a \ln\left(\frac{v}{v_0}\right) + b \ln\left(\theta(t)\frac{v_0}{D_C}\right), \qquad (1)$$

where $v_0$ is a reference velocity, $\mu_0$ is the reference friction coefficient corresponding to $v_0$, $D_C$ is known as the memory distance, which is the sliding distance a population of contacts must slide to refresh itself, and $\theta$ is called the "state variable," which is a function of time. The state variable represents the "state" of the contact and is modeled using different relations depending on the specific RSF model being followed. The behavior described by the second term in Eq. (1) is the "direct effect," whose physical basis lies in the fact that thermal energy assists sliding more strongly at slower velocities [22]. The behavior described by the third term is the "evolution effect," in which $\theta$ evolves with the contact time. The factors $a$ and $b$ represent the magnitudes of the direct and evolution effects, respectively.

One manifestation of evolution is the logarithmic increase of static friction $F_s$ with hold time (i.e., the time of stationary contact). This "aging" effect has been observed in many systems, including in rock friction experiments for hold times from 0.1 to $10^5$ s [1,2,5]. Two mechanisms of aging have been proposed, generally referred to as "contact quantity" and "contact quality." The former refers to an increase in the real contact area, leading to increased friction [23,24], including creep. The latter refers to an increase in friction without changing contact

 

area, due instead to chemical bonding or better atomic registry [25].

Previous experiments [26] and simulations [27,28] for single asperities showed that chemical bonding can contribute to aging at the nanoscale for amorphous silica-silica nanocontacts. Silica is of particular interest for such experiments because silicate minerals are the most abundant constituents of Earth's crust, where earthquakes primarily occur. Faults in the earth are also often mineralized with silica due to flow of silica-rich fluids through fault zones, even when the fault-bounding rocks are not siliceous, and amorphous silica has similar frictional behavior to that of silicate rocks [26,29]. The aging behavior was determined through slide-hold-slide (SHS) experiments [26] with an atomic force microscope (AFM) and subsequent first-principles calculations and Monte Carlo simulations [27,28]. In the experiments, the silica substrates were first treated with piranha solution, which leaves them hydrophilic due to surface hydroxylation. The tip of the AFM is then translated across the substrate, held stationary for some time, then slid again. Hold times were varied from 0.1 to 100 s, and a logarithmic increase of the friction drop $\Delta F$, defined as the difference between the static friction force and the kinetic friction force, was observed. The results indicate that one component of conventional RSF laws—the aging law—can apply well to these nanoscale contacts. This aging was observed in the absence of contact area growth. Instead, they proposed that aging resulted from the formation of chemical bonds at the tip-sample interface. The calculations of Liu *et al.* showed that the bonding occurs through the condensation reaction Si-OH + Si-OH → Si-O-Si + $H_2O$, where the Si-OH groups are present on the tip and substrates surfaces. This group also showed that the number of bonds and thus friction varied with contact time nearly logarithmically over timescales comparable to the experiments [27,28]. Our subsequent AFM study of stick-slip events and the load and time dependence of aging further corroborated these theoretical studies [30,31]. These studies establish an understanding of interfacial chemical bond-induced (ICBI) friction for silica-silica single-asperity interfaces.

Though conventional RSF laws were originally established to describe frictional behavior of macroscale contacts, which are composed of many asperities, recent studies have shown that RSF laws also well describe friction data for microscale contacts composed of only a few asperities, such as in microelectromechanical systems [32–34]. Since the recent results described above show that the aging law applies at the nanoscale, it is natural to ask whether the full conventional RSF formalism can be applied to nanoscale single-asperity contacts.

To address this question, we propose a physically based model for RSF behavior of single-asperity contacts based on the thermally activated Prandtl-Tomlinson (PTT) model [35,36], a fundamental theory that describes atomic-scale stick-slip friction (Fig. 1). In the PTT model, the loading point velocity, which is the loading velocity of the piezoelectric scanner controlling the base of the AFM cantilever, remains constant during stick-slip events. Atomic stick-slip tip motion across a crystalline substrate is considered as a series of repeated jumps over potential energy barriers. The system is composed of the contact, the tip, and the cantilever, and the energy barrier is determined by the combination of the tip-sample interaction energy and the elastic potential energy due to deformation of the system. Sticking occurs when the system remains in an energy well; slip occurs when the system jumps over a barrier. The PTT model predicts that external applied lateral force $F_L$ reduces the energy barrier $\Delta E$ according to $\Delta E = (1/\beta)(F_L^* - F_L)^{3/2}$ [36], where $\beta$ depends on the shape of the energy landscape, and $F_L^*$ is the lateral force needed to make the energy barrier vanish at zero temperature. Based on a master equation describing the evolution of the probability of the system residing in an energy well with time [35,36], a theoretical derivation gives

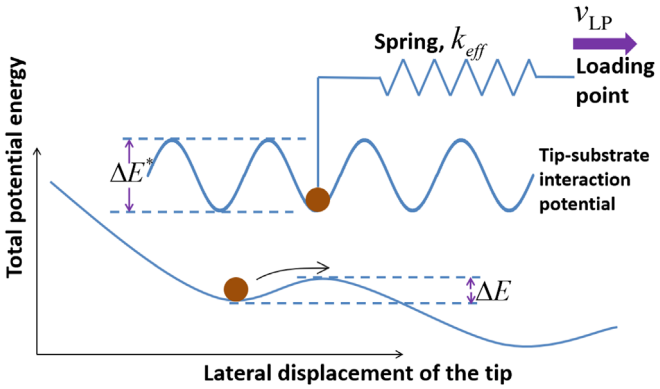


FIG. 1. Schematic of the PTT model. The total potential energy is the summation of the tip-substrate interaction potential and the spring potential. In the top inset, the tip-spring model is shown, with spring stiffness $k_{\mathrm{eff}}$ and loading point velocity $v_{\mathrm{LP}}$. The tip-substrate interaction potential is modeled to be sinusoidal, although the focus is on a single potential well with barrier height $\Delta E^*$. For the total potential energy, the energy barrier under an applied lateral force is $\Delta E$. For nonzero temperatures, thermal fluctuations assist the system in jumping over the energy barrier even when $\Delta E > 0$.

$$\frac{1}{\beta k_B T}(F_L^* - F_L)^{3/2} = 2.3 \log\left(\frac{v_c}{v_{\mathrm{LP}}}\right) - 1.15 \log\left(1 - \frac{F_L}{F_L^*}\right), \tag{2}$$

where $v_c = 2 f_0 \beta k_B T/(3 k_{\mathrm{eff}} F_L^{*1/2})$ is a constant. Here, $F_L$ represents the maximum lateral force in each stick-slip event (i.e., $F_s$), $k_{\mathrm{eff}}$ is the effective lateral stiffness of the system, $f_0$ is the characteristic vibrational frequency in the potential, and $v_{\mathrm{LP}}$ is the loading point velocity. At low $v_{\mathrm{LP}}$, $F_L$ first increases with $\log(v_{\mathrm{LP}})$ almost linearly, and then reaches a plateau (i.e.,$F_L^*$).

An intuitive explanation of these velocity dependences of friction is as follows: at nonzero temperatures, thermal fluctuations give the system a finite probability of jumping over the barrier before the barrier is reduced to zero by the applied lateral force (black curved arrow, Fig. 1). The larger the $v_{\mathrm{LP}}$, the fewer the chances for thermal energy to assist in jumping over the barrier; with less assistance from thermal fluctuations, the maximum applied lateral force needed to overcome the barrier will increase, leading to larger friction. When $v_{\mathrm{LP}}$ is large enough, thermal fluctuations have no further effect on the jumping of the system, resulting in an athermal, velocity-independent regime of friction.

When $v_{\mathrm{LP}}$ is small (and thus $F_L \ll F_L^*$), a linear approximation can be made: $\Delta E = \lambda(F_L^* - F_L)$ [35], where $\lambda$ depends on the shape of the energy landscape. We define $\Delta E^* = \Delta E(F_L = 0) = \lambda F_L^*$.

Under this linear approximation, theoretical analysis gives

$$F_L(v_{\mathrm{LP}}) = F_L^* + 2.3\frac{k_B T}{\lambda}\log\left(\frac{v_{\mathrm{LP}} k_{\mathrm{eff}}\lambda}{f_0 k_B T}\right) \propto \log(v_{\mathrm{LP}}). \quad (3)$$

Equation (3) could also be obtained by performing a Taylor expansion of $(F_L^* - F_L)^{3/2}$ and ignoring the $\log[1-(F_L/F_L^*)]$ term in Eq. (2) under the assumption that $F_L \ll F_L^*$.

Since we do not reach the plateau regime in our experiments, when we discuss the velocity dependence of friction, we will henceforth use the linear approximation, Eq. (3), rather than Eq. (2).

We comment that although the interaction potential between the tip and the substrate in the original PTT model is assumed to be periodic (i.e., the substrates are crystalline), the derivations of Eqs. (2) and (3) actually could apply to just one energy barrier (see the derivations in Refs. [35,36]). Another condition of the PTT model is that the contact does not age.

For nonaging contacts with amorphous substrates, the kinetic friction (if defined as the averaged lateral force among a series of nonuniform stick-slip events) also increases with loading point velocity logarithmically, as indicated by Eq. (4) (see our derivations in Supplemental Material, Sec. 5 [37]):

$$F_k = \frac{\overline{\Delta E^*}}{\lambda} - \frac{k_{\mathrm{eff}}}{2}d + 2.3\frac{k_B T}{\lambda}\log\left(\frac{v_{\mathrm{LP}} k_{\mathrm{eff}}\lambda}{f_0 k_B T}\right), \quad (4)$$

where $\overline{\Delta E^*}$ is the averaged $\Delta E^*$ among all energy barriers along the sliding trace and $d$ is the averaged slip distance of each stick-slip event. Both $\overline{\Delta E^*}$ and $d$ are constants, determined by the structure of the substrate and interfacial interactions, and independent of $v_{\mathrm{LP}}$.

Therefore, we apply the PTT model to amorphous substrates here to describe static friction and kinetic friction.

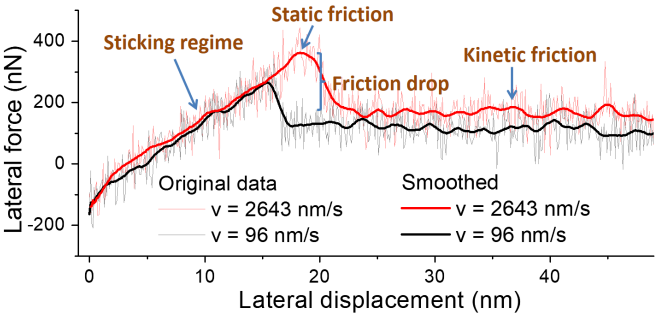


FIG. 2. Lateral force versus lateral displacement for two loading point velocities. Both original data and smoothed curves through the data are shown. The sticking regime, static friction, kinetic friction, and friction drop are also shown. At the higher loading point velocity (red data), kinetic friction and static friction are both larger than at lower velocity (gray data and black smoothed curve). Relative humidity 45%, temperature 24 °C, applied normal load 127 nN, adhesion 583 nN, hold time 4.64 s.

The key ingredient that must be added to the PTT model to account for aging is to allow the intrinsic energy barrier $\Delta E^*$ to increase with time. Recent work on the strengthening of crystalline nanocontacts by Mazo *et al.* [46] indeed incorporated an increase of the energy barrier with time. For reasons discussed further below, we modify the PTT model in a different manner than in Ref. [46]. In our static aging tests (i.e., SHS tests) for single-asperity silica-silica contacts [26,30], the loading point velocity and the hold time are always large enough that the hold time (about 1–5 s) is much greater than the time during which the lateral force is progressively increasing before the tip slips (about 0.01–0.15 s). Thus, most of the aging occurs before lateral loading starts (the lateral loading refers to the sticking regime, where the lateral force progressively increases with time and lateral displacement; see Fig. 2). We thus treat $\Delta E^*$ during lateral loading as constant. Thus, we can directly use the PTT model for our contacts (one condition of the PTT model is that $\Delta E^*$ and thus $F_L^*$ are independent of time during the lateral loading process).

Since $F_L^*$ is the applied lateral force needed for the energy barrier to vanish at zero temperature, we assume that $F_L^*$ is proportional to the number of interfacial chemical bonds formed. According to previous studies on nanoscale ICBI aging, the number of interfacial chemical bonds increases logarithmically over a wide range of hold times [26,27,30]. Therefore, $F_L^*(t) = F_{L,0}^* + B\log(t)$, where both $F_{L,0}^*$ and $B$ are constants. After a hold time $\tau$ has elapsed, $F_L^*(\tau) = F_{L,0}^* + B\log(\tau)$. Since $\lambda$ depends on the shape of the energy landscape, it will depend on $\tau$, giving

$$F_L(v_{\mathrm{LP}}, \tau) = F_{L,0}^* + B\log(\tau) + 2.3\frac{k_B T}{\lambda(\tau)}\log\left(\frac{v_{\mathrm{LP}} k_{\mathrm{eff}}\lambda(\tau)}{f_0 k_B T}\right). \quad (5)$$

Equation (5) is thus a physically based RSF relation for nanoscale single-asperity contacts, where an aging effect

(i.e., terms depending on time) is incorporated into the PTT model. We call this the thermally activated Prandtl-Tomlinson with chemical aging (PTTCA) model.

We note that our Eq. (5) is similar to Eq. (8) in Mazo *et al.* [46], a recent model for nanocontacts where time-dependent strengthening of the contact (i.e., aging) was incorporated into the PTT model for the first time. There are several key differences in the two models. First, the model of Mazo *et al.* is formulated to describe atomic stick-slip behavior (i.e., for a crystalline sample), although like our model, it might be extended to nonperiodic systems. Conceptually, the model of Mazo *et al.* is inspired by observations supporting atomic attrition of the contact, i.e., a change in contact quantity, whereas our aging is due to interfacial chemical bond formation, i.e., a change of contact quality. Second, our model considers static aging during the hold period that occurs before lateral loading starts, while Mazo *et al.* describe the aging that occurs during the periodic lateral loading of atomic stick-slip behavior. In our model, the evolution of the contact in the stick phase during lateral loading is ignored, making application of the PTT model during lateral loading feasible. In contrast, Mazo *et al.* assume that the first time derivatives of certain parameters such as the interaction potential are slowly varying. Third, in our work, aging is logarithmic with time, while in Mazo *et al.*, aging saturates exponentially with time. The latter has the advantage of incorporating the expected saturation of aging [27,47], but it is phenomenological. Though our logarithmic dependence only applies to hold times well below saturation, it has a physical basis as discussed above. Thus, while both models integrate aging with thermally assisted slip, they are aimed at explaining different manifestations of aging and accordingly use different assumptions, apply for different time ranges, and produce different results.

The PTTCA model indicates that the conventional RSF laws must be modified in at least two respects at the nanoscale. The first modification is the physical meaning of velocity in direct effect. In conventional RSF laws, the velocity refers to the velocity of the sliding block, while for the PTTCA model, it refers to the loading point velocity. This difference arises because in macroscale experiments on multiasperity frictional interfaces, there is no true static state (i.e., zero sliding velocity) for the block during a hold in a SHS test since the external lateral force on the block is always close to the sliding friction force, resulting in slow sliding of the block. Therefore, the block velocity $v$ in Eq. (1) will always be nonzero, so there is no problem with using $v$ to determine the direct effect [i.e., $\log(v)$ will not diverge]. However, for ICBI friction for nanoscale single-asperity contacts, the AFM tip can stick to the substrate with zero motion, even with a large applied lateral force (see the linearity of the sticking regime in Fig. 2, indicating no partial slip or appreciable tip motion during stick; even clearer linear sticking regimes with less noise are seen in our previous work [30]). Zero motion is also shown by multiple molecular dynamics simulations of contacts, wherein the interface is completely stable during sticking [28,48,49]. Therefore, the tip velocity can be zero during lateral loading, and $\log(v)$ can diverge. In contrast, since $v_{\mathrm{LP}}$ is the loading point velocity and is always nonzero in the jumping-over-barrier process, we thus avoid this problem.

The second modification is in the manner in which the direct and evolution effects combine. In conventional RSF laws [Eq. (1)], since parameters $a$ and $b$ are constants, the direct and evolution effects combine linearly. However, in

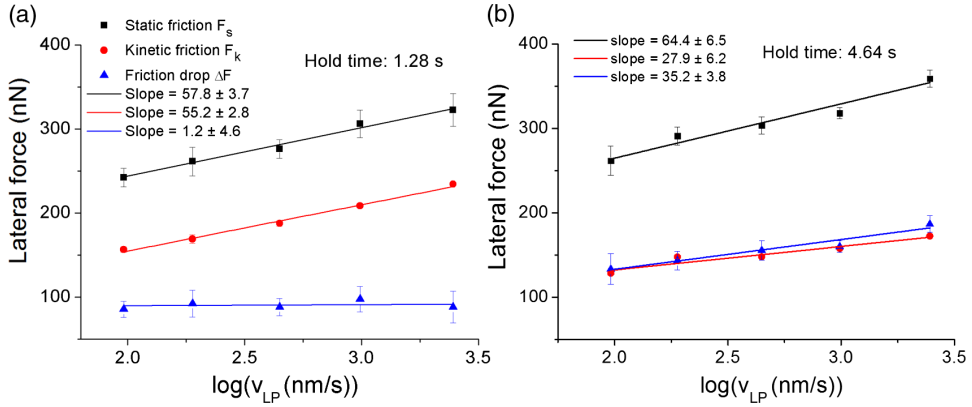


FIG. 3. Lateral force versus loading point velocity for different hold times. (a) Static friction, kinetic friction, and friction drop versus loading point velocity for a 1.28 s hold time. Both static friction and kinetic friction show a logarithmic increase with velocity. The friction drop in this case is almost independent of velocity since the slopes of the trends of static friction and kinetic friction with log of loading point velocity are the same. (b) Static friction, kinetic friction, and friction drop versus loading point velocity for a 4.64 s hold time. Static friction, kinetic friction, and friction drop all increase with velocity logarithmically. In this case, the slopes of the trends of static friction and kinetic friction with the log of the loading point velocity are different, resulting in a dependence of friction drop on velocity. For both (a) and (b), velocity is varied randomly to exclude systematic error. The conditions are the same as those in Fig. 2, with the same AFM tip used.

the PTTCA model [Eq. (5)], since the prefactor of the direct effect, $2.3[k_BT/\lambda(\tau)]$, is a function of time, the direct and evolution effects are nonlinearly convoluted.

We now present experimental evidence for the logarithmic increase of friction with loading point velocity and for the nonlinear combination of the direct and evolution effects. Figure 2 shows how we measure $F_s$, $F_k$, and $\Delta F$. Measurements for two different values of $v_{\mathrm{LP}}$ are shown. Despite having the same hold time, $F_s$ is clearly higher for the higher $v_{\mathrm{LP}}$. Figure 3 shows how these three quantities vary over a range of $v_{\mathrm{LP}}$ for two different hold times. For a 1.28 s hold time, $F_s$ and $F_k$ both increase with $\log(v_{\mathrm{LP}})$ linearly. Their slopes agree within measurement uncertainty [Fig 3(a)]. The logarithmic increase of $F_s$ with $v_{\mathrm{LP}}$ corroborates the direct effect term in Eq. (5). For this hold time, $\Delta F$ is nearly independent of velocity. For a 4.64 s hold time [Fig. 3(b)], the slopes of $F_s$ and $F_k$ vs $\log(v_{\mathrm{LP}})$ differ more, leading to a nonzero slope of $\Delta F$ vs $\log(v_{\mathrm{LP}})$. The different slopes of $F_s$ with $\log(v_{\mathrm{LP}})$ and $F_k$ with $\log(v_{\mathrm{LP}})$ indicate that the combination of the direct effect and the evolution effect is nonlinear, as discussed further below.

In Fig. 3(b), during steady sliding, since the velocities are relatively large (greater than ~100 nm/s), the evolution effect is largely suppressed and relatively few interfacial chemical bonds form during sliding (more details on the suppression of evolution effect during sliding will be published elsewhere). Assuming that the apparently steady sliding observed at large velocities is actually a series of irregular stick-slip events due to the amorphous atomic structure of the substrate and tip, which is obscured due to the large tip radius (~125 nm, as shown in Supplemental Material Sec. 1 [37]) and noise, we could use the PTT model [Eq. (4)] to describe $F_k$ at these high velocities (see more details in Supplemental Material Sec. 5 [37]). If the direct and evolution effects were linearly combined, then the prefactor of the direct effect, which is the rate of increase of friction with, would be independent of the magnitude of the evolution effect. Thus, the rate of increase of $F_s$ and $F_k$ with $\log(v_{\mathrm{LP}})$ would be the same. This contradicts our observations of different slopes of $F_s$ and $F_k$ vs $\log(v_{\mathrm{LP}})$ in Fig. 3(b), indicating that the assumption that the direct and evolution effects combine linearly is false. Therefore, in Fig. 3(b), the combination of the direct and evolution effects is nonlinear, consistent with the PTTCA model.

We comment that in previous studies on nanoscale ICBI friction [26,30], $\Delta F$ was taken to represent the magnitude of aging. However, the independence of $\Delta F$ on $v_{\mathrm{LP}}$ in Fig. 3(a) indicates that $\Delta F$ is not a good measure for aging if $v_{\mathrm{LP}}$ varies; in such a case, a more comprehensive analysis is required to separate aging effects from rate effects. The PTTCA model presented here allows such analysis to be conducted.

In conclusion, we establish the PTTCA model, which is a physically based RSF relation for nanoscale single-asperity contacts exhibiting chemical aging. In this model, the velocity for the direct effect is not the velocity of the tip, but the loading point. The direct and evolution effects can combine nonlinearly. The PTTCA model is consistent with our experimental observations from aging tests, which show that for a given hold time, static friction increases with loading point velocity logarithmically. Also, the nonlinear combination of the direct and evolution effects is consistent with our experimental finding that the rate of increase of static friction and kinetic friction with the log of loading point velocity can differ at higher velocities. These results show how conventional RSF laws can be modified to establish a physically based friction relation for nanoscale contacts. It also extends the PTT model to amorphous surfaces.

We thank Nitya N. Gosvami for useful discussions. We acknowledge funding from the National Science Foundation under Grants No. EAR-1141142, No. EAR-1141882, and No. EAR 15-50112.

K. T. performed experiments, obtained and analyzed the data, constructed models, and wrote this manuscript with input from all coauthors.

*Present address: School of Chemical and Biomolecular Engineering, Cornell University, Ithaca, NY 14853, USA.
†carpick@sas.upenn.edu

[1] J. H. Dieterich, Time-dependent friction in rocks, J. Geophys. Res. **77**, 3690 (1972).
[2] J. H. Dieterich, Modeling of rock friction: 1. Experimental results and constitutive equations, J. Geophys. Res. **84**, 2161 (1979).
[3] J. R. Rice and A. L. Ruina, Stability of steady frictional slipping, J. Appl. Mech. **50**, 343 (1983).
[4] N. M. Beeler, T. E. Tullis, and J. D. Weeks, The roles of time and displacement in the evolution effect in rock friction, Geophys. Res. Lett. **21**, 1987 (1994).
[5] C. Marone, Laboratory-derived friction laws and their application to seismic faulting, Annu. Rev. Earth Planet Sci. **26**, 643 (1998).
[6] P. Berthoud, T. Baumberger, C. G'Sell, and J.-M. Hiver, Physical analysis of the state- and rate-dependent friction law: Static friction, Phys. Rev. B **59**, 14313 (1999).
[7] T. Baumberger, P. Berthoud, and C. Caroli, Physical analysis of the state- and rate-dependent friction law. II. Dynamic friction, Phys. Rev. B **60**, 3928 (1999).
[8] M. F. Linker and J. H. Dieterich, Effects of variable normal stress on rock friction: Observations and constitutive equations, J. Geophys. Res. **97**, 4923 (1992).
[9] J. H. Dieterich, *Mechanical Behavior of Crustal Rocks: The Handin* Vol. 24 (American Geophysical Union, Washington, DC, 1981), p. 103.
[10] D. D. Kosloff and H. P. Liu, Reformulation and discussion of mechanical behavior of the velocity-dependent friction law proposed by Dieterich, Geophys. Res. Lett. **7**, 913 (1980).
[11] J. H. Dieterich, Modeling of rock friction: 2. Simulation of preseismic slip, J. Geophys. Res. **84**, 2169 (1979).

[12] J. H. Dieterich, *Time-Dependent Friction and the Mechanics of Stick-Slip* (Springer, New York, 1978), p. 790–806.
[13] A. Ruina, Slip instability and state variable friction laws, J. Geophys. Res. **88**, 10359 (1983).
[14] A. L. Ruina, Ph.D. thesis, Brown University, 1982, p. 1982.
[15] C. Marone, C. B. Raleigh, and C. Scholz, Frictional behavior and constitutive modeling of simulated fault gouge, J. Geophys. Res. **95**, 7007 (1990).
[16] F. Heslot, T. Baumberger, B. Perrin, B. Caroli, and C. Caroli, Creep, stick-slip, and dry-friction dynamics: Experiments and a heuristic model, Phys. Rev. E **49**, 4973 (1994).
[17] J. R. Rice, Constitutive relations for fault slip and earthquake instabilities, Pure Appl. Geophys. **121**. 443 (1983).
[18] T. E. Tullis and J. D. Weeks, Constitutive Behavior and Stability of Frictional Sliding of Granite, in *Friction and Faulting* (Springer, New York, 1987), p. 383–414.
[19] A. D. Corwin and M. P. de Boer, Frictional aging and sliding bifurcation in monolayer-coated micromachines, J. Microelectromech. Syst. **18**, 250 (2009).
[20] A. D. Corwin and M. P. de Boer, Frictional aging, de-aging, and re-aging in a monolayer-coated micromachined interface, Phys. Rev. B **81**, 174109 (2010).
[21] S. S. Shroff, N. Ansari, W. R. Ashurst, and M. P. de Boer, Rate-state friction in microelectromechanical systems interfaces: Experiment and theory, J. Appl. Phys. **116**, 244902 (2014).
[22] J. R. Rice, N. Lapusta, and K. Ranjith, Rate and state dependent friction and the stability of sliding between elastically deformable solids, J. Mech. Phys. Solids **49**, 1865 (2001).
[23] F. Bowden and D. Tabor, The area of contact between stationary and between moving surfaces, Proc. R. Soc. A **169**, 391 (1939).
[24] I. Szlufarska, M. Chandross, and R. W. Carpick, Recent advances in single-asperity nanotribology, J. Phys. D **41**, 123001 (2008).
[25] S. Li, Q. Li, R. W. Carpick, P. Gumbsch, X. Z. Liu, X. Ding, J. Sun, and J. Li, The evolving quality of frictional contact with graphene, Nature (London) **539**, 541 (2016).
[26] Q. Li, T. E. Tullis, D. Goldsby, and R. W. Carpick, Frictional ageing from interfacial bonding and the origins of rate and state friction, Nature (London) **480**, 233 (2011).
[27] Y. Liu and I. Szlufarska, Chemical Origins of Frictional Aging, Phys. Rev. Lett. **109**, 186102 (2012).
[28] A. Li, Y. Liu, and I. Szlufarska, Effects of interfacial bonding on friction and wear at silica/silica interfaces, Tribol. Lett. **56**, 481 (2014).
[29] J. Weeks, N. Beeler, and T. Tullis, Glass is like a rock, EOS Trans, Am. Geophys. Union **72**, 457 (1991).
[30] K. Tian, N. N. Gosvami, D. L. Goldsby, Y. Liu, I. Szlufarska, and R. W. Carpick, Load and Time Dependence of Interfacial Chemical Bond-Induced Friction at the Nanoscale, Phys. Rev. Lett. **118**, 076103 (2017).
[31] K. Tian, N. N. Gosvami, D. L. Goldsby, and R. W. Carpick, Stick-slip instabilities for interfacial chemical bond-induced friction at the nanoscale, J. Phys. Chem. B **122**, 991 (2018).
[32] S. S. Shroff and M. P. de Boer, Full assessment of micromachine friction within the rate-state framework: Experiments, Tribol. Lett. **63**, 1 (2016).
[33] S. S. Shroff and M. P. de Boer, Direct observation of the velocity contribution to friction in monolayer-coated micromachines, Extreme Mech. Lett. **8**, 184 (2016).
[34] S. S. Shroff and M. P. de Boer, Constant velocity high force microactuator for stick-slip testing of micromachined interfaces, J. Microelectromech. Syst. **24**, 1868 (2015).
[35] E. Gnecco, R. Bennewitz, T. Gyalog, Ch. Loppacher, M. Bammerlin, E. Meyer, and H.-J. Güntherodt, Velocity Dependence of Atomic Friction, Phys. Rev. Lett. **84**, 1172 (2000).
[36] E. Riedo, E. Gnecco, R. Bennewitz, E. Meyer, and H. Brune, Interaction Potential and Hopping Dynamics Governing Sliding Friction, Phys. Rev. Lett. **91**, 084502 (2003).
[37] See Supplemental Material at http://link.aps.org/supplemental/10.1103/PhysRevLett.120.186101 for details of sample preparation, tip characterization, derivations of equations, another set of data, and other discussions, which includes Refs. [38–45].
[38] L. Dongmo, J. S. Villarrubia, S. N. Jones, T. B. Renegar, M. T. Postek, and J. F. Song, Experimental test of blind tip reconstruction for scanning probe microscopy, Ultramicroscopy **85**, 141 (2000).
[39] B. V. Derjaguin, V. M. Muller, and Y. P. Toporov, Effect of contact deformations on the adhesion of particles, J. Colloid Interface Sci. **53**, 314 (1975).
[40] T. H. Elmer, Porous and reconstructed glasses, ASM Int. Eng. Mater. Handb. **4**, 427 (1991).
[41] J. E. Sader, J. W. M. Chon, and P. Mulvaney, Calibration of rectangular atomic force microscope cantilevers, Rev. Sci. Instrum. **70**, 3967 (1999).
[42] E. Meyer, H. J. Hug, and R. Bennewitz, *Scanning Probe Microscopy: The Lab on a Tip* (Springer, New York, 2004).
[43] C. P. Green, H. Lioe, J. P. Cleveland, R. Proksch, P. Mulvaney, and J. E. Sader, Normal and torsional spring constants of atomic force microscope cantilevers, Rev. Sci. Instrum. **75**, 1988 (2004).
[44] R. Lüthi, E. Meyer, H. Haefke, L. Howald, W. Gutmannsbauer, M. Guggisberg, M. Bammerlin, and H.-J. Güntherodt, Nanotribology: An UHV-SFM study on thin films of $C_{60}$ and AgBr, Surf. Sci. **338**, 247 (1995).
[45] A. Craciun, J. Gallani, and M. Rastei, Stochastic stick-slip nanoscale friction on oxide surfaces, Nanotechnology **27**, 055402 (2016).
[46] J. J. Mazo, D. Dietzel, A. Schirmeisen, J. G. Vilhena, and E. Gnecco, Time Strengthening of Crystal Nanocontacts, Phys. Rev. Lett. **118**, 246101 (2017).
[47] J. B. Walsh and D. L. Goldsby, Modeling the mechanics of rate and state friction with linear viscoelasticity, J. Geophys. Res. **113**, B09408 (2008).
[48] X.-Z. Liu, Z. Ye, Y. Dong, P. Egberts, R. W. Carpick, and A. Martini, Dynamics of Atomic Stick-Slip Friction Examined with Atomic Force Microscopy and Atomistic Simulations at Overlapping Speeds, Phys. Rev. Lett. **114**, 146102 (2015).
[49] Q. Li, Y. Dong, D. Perez, A. Martini, and R. W. Carpick, Speed Dependence of Atomic Stick-Slip Friction in Optimally Matched Experiments and Molecular Dynamics Simulations, Phys. Rev. Lett. **106**, 126101 (2011).

*Correction:* The previously published Figure 1 contained an axis-label error and has been replaced.